

Nanoscale

Accepted Manuscript



This is an *Accepted Manuscript*, which has been through the Royal Society of Chemistry peer review process and has been accepted for publication.

Accepted Manuscripts are published online shortly after acceptance, before technical editing, formatting and proof reading. Using this free service, authors can make their results available to the community, in citable form, before we publish the edited article. We will replace this *Accepted Manuscript* with the edited and formatted *Advance Article* as soon as it is available.

You can find more information about *Accepted Manuscripts* in the [Information for Authors](#).

Please note that technical editing may introduce minor changes to the text and/or graphics, which may alter content. The journal's standard [Terms & Conditions](#) and the [Ethical guidelines](#) still apply. In no event shall the Royal Society of Chemistry be held responsible for any errors or omissions in this *Accepted Manuscript* or any consequences arising from the use of any information it contains.

COMMUNICATION

Micromotor Based on Polymer Single Crystal and Nanoparticle: Toward Functional Versatility†

Cite this: DOI: 10.1039/x0xx00000x

Mei Liu,^a Limei Liu,^a Wenlong Gao,^a Miaoda Su,^a Ya Ge,^a Lili Shi,^a Hui Zhang,^a Bin Dong*^a and Christopher Y. Li*^b

Received 00th January 2012,

Accepted 00th January 2012

DOI: 10.1039/x0xx00000x

www.rsc.org/

We report a multifunctional micromotor fabricated by self-assembly technique using multifunctional materials, i.e. polymer single crystals and nanoparticles, as basic building blocks. Not only can this micromotor achieve autonomous and directed movement, it also possesses unprecedented functions, including enzymatic degradation-induced micromotor disassembly, sustained release and molecular detection.

Researches on micromotors represent the key step towards the future development of more complicated micromachines.¹⁻⁵ To this end, many efforts have been exerted in the fabrication of micromotors, resulting in the development of a variety of different forms of micromotors.⁶⁻¹⁴ Representative examples include segmented nanorod comprising different metals,^{7-9,14} microspheres containing asymmetric surface compartment,¹⁵⁻¹⁷ and microtubes made of layer-by-layer deposited metals.^{10,13} The motion of these developed micromotors can generally be achieved by utilizing the catalytic or reactive part inside micromotors, which can generate propulsion forces through catalytic or chemical reaction upon addition of a fuel.

On the other hand, functions that can be achieved by these micromotors are essential for the future of micromotor research. It has been previously demonstrated that, through molecular recognition or magnetic interaction, micromotors can be used for cargo transportation,^{9,11} cell separation,¹³ targeted delivery,¹⁸ controlled release,^{19,20} etc. Recently, Wang and Sanchez et al. have reported the utilization of micromotors to remove oil droplets in water or clean out an organic pollutant in solution for environmental remediation.²¹⁻²³ Micromotor can also be used as a platform for sensing,²⁴ such as motion based sensors for specific ions or DNAs.^{25,26}

Despite these progresses, there are still challenges in the field of micromotors. To meet the future requirement for the diverse applications involving micromotors and move forward toward the ultimate goal of fabricating more sophisticated micromachines, it is desirable to develop micromotors that possess multiple functions.²⁷ Current strategies to fabricate micromotors are generally based on template synthesis (e.g. using filter membranes as the template materials) or microfabrication methods (e.g. photolithography, sputtering, etc.). Hence, fabricating multifunctional micromotors requires incorporation of multiple functional parts into a single

micromotor.²⁷ Since the fabrication of micromotor itself already involves several steps, the introduction of more functional parts will inevitably increase the fabrication complexity. To overcome this problem, it is preferable to utilize materials that possess multiple functions.

By utilizing a scalable self-assembly method, we have recently developed a micromotor system based on nanoparticle-decorated polymer single crystal. These polymer single crystal-based micromotors can achieve autonomous movement in H₂O₂ solution.²⁸ In this paper, we show that polymer single crystal-based micromotors can address the aforementioned challenge. Because of the versatility in functionalities originated from both polymer single crystals and nanoparticles (e.g. biodegradability, catalytic property and surface plasmon resonance (SPR)), the resulting micromotors exhibit multiple functions, including commonly reported autonomous movement, sustained release and molecular detection. Furthermore, due to the biodegradable property of the polymer, the micromotors can be enzymatically disassembled.

The micromotor is obtained by self-assembly method following steps shown in Fig. S1 (ESI†). In brief, a biodegradable polymer, i.e. polycaprolactone, containing end functional thiol groups (denoted as PCL-SH) is first solution crystallized to form hexagonal shaped polymer single crystals (8 nm thick) bearing surface thiol groups (Fig. S1, ESI†),²⁸⁻³⁰ onto which, a layer of 6 nm sized gold nanoparticles (AuNPs) is immobilized through gold-thiol bond (Fig. S2).³¹ Silver nanoparticles (AgNPs) are then deposited by a silver enhancement method utilizing the pre-adsorbed AuNPs as the seeds.^{32,33} Fig. 1a shows the low magnification TEM image of the resulting AgNP-decorated polycaprolactone single crystal (denoted as Ag-PCL) obtained after 3 min silver enhancement. As can be seen from the enlarged TEM image (Fig. 1b), the deposited AgNPs are irregular in shape, and the average size of the nanoparticle is around 45 nm (the size distribution histogram is shown in Fig. S3, ESI†). Fig. 1c shows the high resolution TEM image indicating a lattice spacing of about 0.236 nm, which corresponds to the (111) plane of silver. By controlling the silver enhancement time, the size and amount of deposited AgNP can be finely tuned (Fig. S2, ESI†), which is consistent with the results shown in the literatures.³⁴ We have further studied the changes in surface plasmon resonance (SPR) band of this polymer/nanoparticle ensemble using UV-Vis

spectroscopy. The SPR band (Fig. S4, ESI†) shifted from 520 nm in the case of 6 nm AuNP decorated polycaprolactone single crystal

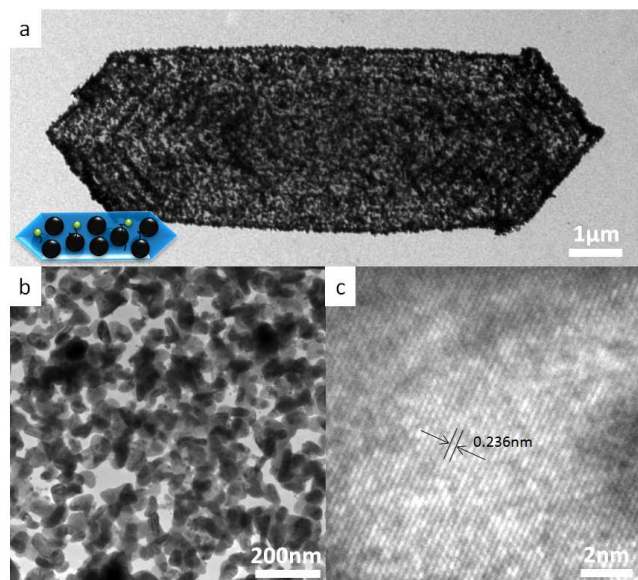


Fig. 1 (a-b) TEM images of Ag-PCL at different magnifications. (c) High resolution TEM image showing the lattice structure of AgNP (111).

(denoted as Au-PCL), which corresponds to the characteristic peak for AuNP to approximately 450 nm in the case of Ag-PCL (the peak width is also significantly broadened), which is the typical band for AgNP,³⁵ indicating the successful deposition of AgNP. In addition, the thickness of Ag-PCL was further examined using atomic force microscopy (AFM) to be around 90 nm (Fig. S5, ESI†). The dimension of Ag-PCL is thus approximately $11 \mu\text{m} \times 3.5 \mu\text{m} \times 90 \text{ nm}$ (length/width/thickness). Current Ag-PCL is based on polymer single crystal. Therefore, the shape and size control of the Ag-PCL can be achieved by adjusting the seeding temperature during crystal growth process. Fig. S6 (ESI†) shows the polymer single crystal grown at different seeding temperature (Fig. S6a-d in ESI†, from 44°C to 47 °C), the size increases gradually and the shape changes from a bar-like structure (Fig. S6a, ESI†) to a hexagonal lamella (Fig. S6d, ESI†).

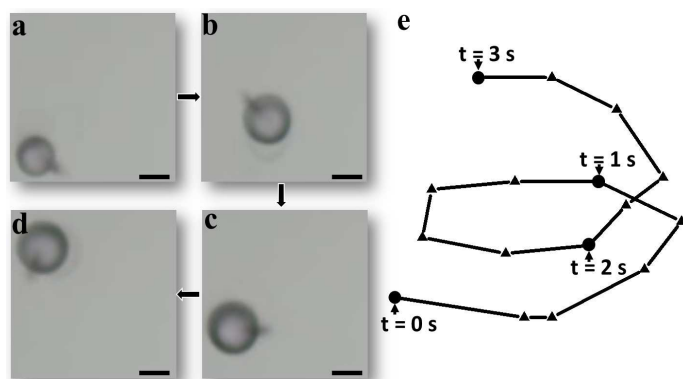


Fig. 2 (a-d) A series of images captured at 1 s interval showing the autonomous movement of an Ag-PCL micromotor. Scale bar: 10 μm . The complete video is shown in the ESI† as Video S1. The corresponding trajectory of this micromotor is shown in (e).

AgNP is well known to be catalytically active.³⁶⁻³⁸ Ag-PCL can therefore decompose H_2O_2 to form oxygen bubbles once placed in

H_2O_2 aqueous solution, which, in turn, provides the direct driving force to propel Ag-PCL. Video S1 (ESI†) shows the autonomous movement of an Ag-PCL in 10% H_2O_2 (in deionized water, no other additives). Fig. 2a-d shows four consecutive images captured from Video S1 (ESI†) at a 1 s interval indicating the circular motion. It can be clearly seen that this micromotor moves rapidly by bubble propulsion. By analyzing the trajectory of this micromotor (depicted in Fig. 2e), the average absolute velocity can thus be calculated to be around 45 $\mu\text{m/s}$. Video S2 (ESI†) shows the large area view of the autonomous movement of Ag-PCL based micromotors in 10% H_2O_2 aqueous solution. These micromotors will not stop moving until the fuel is exhausted (last for $\sim 1 \text{ h}$). By carefully studying the trajectory of each individual micromotor, the average absolute speed can thus be estimated to be approximately 50 $\mu\text{m/s}$, which corresponds to ~ 5 body lengths per second. The micromotor's absolute speed is highly dependent on the concentration of H_2O_2 aqueous solution, which decreases from 50 $\mu\text{m/s}$ in 10% H_2O_2 to about 25 $\mu\text{m/s}$ in 5% H_2O_2 and increases to around 80 $\mu\text{m/s}$ in 15% H_2O_2 (Fig. S7, ESI†). This result is consistent with that shown in the literature.⁷

The applications related to micromotors often require them being fully operational in ionic solution. Since the initially reported segmented nanorod based motor is not suitable for autonomous movement at high ionic strength,⁷ Mei, Sanchez, Schmidt and Wang et al. later developed the microtube based micromotors which have overcome this problem.^{10,13,39,40} In addition, Guan and Wang et al. have recently reported that the magnesium-based micromotor can be self-propelled in salt solution.^{17,41} In our case, since AgNPs still exhibit catalytic activity in the presence of salts,^{36,37} current Ag-PCL based micromotor is capable of moving autonomously in phosphate buffer solution (PBS) containing 10% H_2O_2 (10% H_2O_2 in $1 \times \text{PBS}$), as shown in Video S3 (ESI†). The micromotor velocity is similar to that in 10% H_2O_2 aqueous solution.

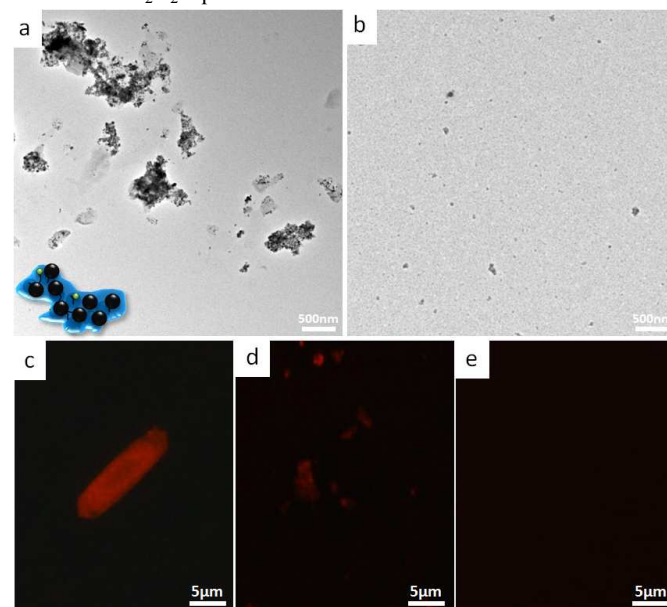


Fig. 3 TEM images showing Ag-PCL after (a) 24 h and (b) 48 h enzymatic disassembly. Fluorescent images of Ag-PCL-RhBITC after (c) 0 h (d) 24 h and (e) 48 h enzymatic disassembly. The excitation wavelength is 546 nm.

Reported micromotor-enabled functions include target transportation,¹⁸ controlled release,^{19,20} etc. It is required, in many cases, that the micromotor is responsive to external stimuli, such as magnetic field or chemicals. Owing to the biodegradability of polycaprolactone,^{42,43} the Ag-PCL micromotor in current study can

be disassembled in the presence of an enzyme. Upon the addition of the lipase from *Pseudomonas cepacia*, the original Ag-PCL shown in Fig. 1a disassembled into smaller pieces after 24 h incubation (Fig. 3a). This enzymatic degradation of polycaprolactone single crystal can be best described as a surface erosion process,⁴⁴ i.e. the hydrolysis of the ester bonds in polycaprolactone progressed perpendicularly from the crystal lateral sides (as shown in Fig. S8, ESI[†]), resulting in the gradual shrinkage in the crystal size. Accompanied by this process, nanoparticles will also be detached from the crystal surface. After 48 h, Ag-PCL is completely disassembled (Fig. 3b). Pumera et al.⁴⁵ have recently reported that micromotor based on heavy metal can corrode in aqueous solution which may pollute the environment. Since enzyme, i.e. catalase, is also capable of decomposing hydrogen peroxide to form water and oxygen, by substituting AgNP with catalase, a micromotor with more bio-friendly disassembly products could be realized. Work along this direction is currently under progress.

Controlled release based on micromotors has previously been realized by applying an external stimulus, such as pH changes¹⁹ and ultrasound.^{20,46} Despite these progresses, few works have reported the sustained release of drug molecules realized by a micromotor,²⁷ particularly over a long period of time, which is advantageous for long term therapeutic applications. By utilizing the enzymatic disassembly of Ag-PCL, sustained release of drug molecules conjugated to the free surface thiol groups²⁸ on Ag-PCL can be achieved. As a proof-of-concept, we covalently link a model drug, i.e. fluorescent Rhodamine B isothiocyanate (RhBITC), onto the surface of Ag-PCL through isothiocyanate and thiol reaction.⁴⁷ Fluorescence microscopy is then utilized to monitor the release process of RhBITC from Ag-PCL. At the beginning, upon 546 nm irradiation, the RhBITC decorated Ag-PCL (abbreviated as Ag-PCL-RhBITC) is clearly visible under fluorescence microscopy showing the characteristic red fluorescence (Fig. 3c). The structure is intact as indicated by the regular hexagonal shape (Fig. 3c), which is consistent with the TEM image (Fig. 1a). Note that there is no background fluorescence at this time indicating RhBITC has not been released. By incubating Ag-PCL-RhBITC in PBS buffer containing lipase from *Pseudomonas cepacia* for 24 h, Ag-PCL-RhBITC is disassembled into smaller pieces, as indicated by the red irregular shaped structure in Fig. 3d, which is consistent with the above TEM observation (Fig. 3a). At the same time, RhBITC is released from Ag-PCL-RhBITC surface into solution, as indicated by the slightly red fluorescence background in Fig. 3d. After 48 h, Ag-PCL-RhBITC is fully disassembled. No shattered pieces of Ag-PCL-RhBITC are observed, indicating the successfully release of all dye molecules (Fig. 3e).

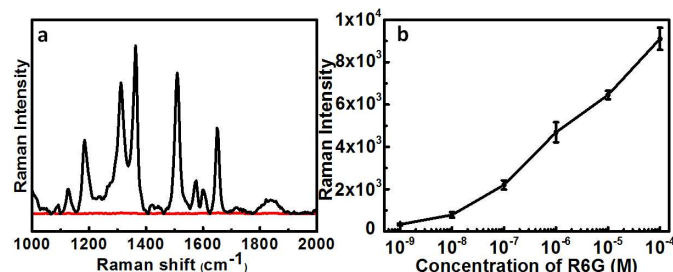


Fig. 4 (a) Raman spectra of R6G solution in the absence of Ag-PCL (red curve) and in the presence of Ag-PCL (black curve). The concentration of R6G is 10^{-4} M. The four characteristic peaks at 1312, 1363, 1509 and 1649 cm^{-1} are clearly visible. The excitation wavelength is 633 nm. (b) A plot showing the intensity of the characteristic peak of R6G at 1363 cm^{-1} versus R6G concentration in solution.

Many living creatures can detect changes in their surrounding environment.²⁴ Inspired by nature, researchers have been seeking ways to incorporate similar function into artificial micromotors.^{25,26} In this study, by utilizing the SPR property from AgNP, we demonstrate that Ag-PCL can be used to directly detect the presence of an analyte in solution based on surface enhanced Raman spectroscopy (SERS). Rhodamine 6G (R6G) is employed as a model analyte for demonstration purpose. In the absence of Ag-PCL, pure R6G solution shows no Raman signal at a concentration of 10^{-4} M (Fig. 4a, red curve). However, in the presence of Ag-PCL, strong characteristic Raman signals from R6G can be observed (Fig. 4a, black curve). The most pronounced peaks at 1312, 1363, 1509 and 1649 cm^{-1} can be assigned to the aromatic stretching vibration of R6G. Moreover, the peak intensity is highly dependent on R6G concentration in solution. The peak intensity at 1363 cm^{-1} decreases gradually from around 9500 in the case of 10^{-4} M to approximately 200 in the case of 10^{-9} M, as shown in Fig. 4b. Since SERS is a quantitative characterization method with well resolved characteristic peaks, which can be used to discriminate not only different chemical species but also their concentrations, we thus believed current strategy provides an alternative way for the further development of micromotor based detection method.

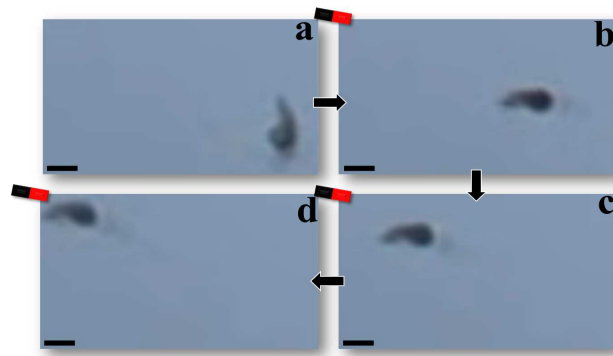


Fig. 5 (a-d) A series of images captured at 1 s interval showing the directed movement of an Ag-PCL micromotor with attached $\text{Fe}_3\text{O}_4\text{NP}$ under an external magnetic field. Scale bar: $10\text{ }\mu\text{m}$. The complete video is shown in the ESI[†] as Video S4.

The functions of current micromotor can be further extended by incorporating more functional nanomaterials, such as magnetic iron oxide nanoparticles ($\text{Fe}_3\text{O}_4\text{NP}$), fluorescent quantum dots, etc., into the system. Here, we take $\text{Fe}_3\text{O}_4\text{NP}$ as an example. $\text{Fe}_3\text{O}_4\text{NP}$ can be easily introduced into Ag-PCL by self-assembly,²⁸ after which, current micromotor becomes magnetically responsive. Because of its ability to maneuver the moving direction of a micromotor, the remote control utilizing external magnetic field^{48,49} is essential to realize some of the key functions offered by micromotors. As demonstrated in Fig. 5a-d and the corresponding Video S4 (ESI[†]), Ag-PCL with attached $\text{Fe}_3\text{O}_4\text{NPs}$, which moves autonomously at the beginning in 10% H_2O_2 aqueous solution, can be quickly steered toward the direction where the magnet is placed with an absolute speed of about $40\text{ }\mu\text{m/s}$.

Conclusions

In conclusion, by utilizing polymer single crystals and nanoparticles as the multifunctional building blocks, a micromotor bearing multifunctions has been successfully fabricated. A self-assembly method was employed to incorporate these building blocks together, and polymer single crystals were used as the platform. Based on the biodegradability from polymers and SPR, catalytic properties from

nanoparticles, the resulting ensemble exhibits a variety of different functions ranging from autonomous movement in buffer solution to detection of a solute, sustained release of a model drug, and enzymatic disassembly. Due to the abundant functions available from both nanoparticles and polymers, the realization of more functions within a single micromotor, such as pH sensing, targeted delivery, can be envisioned.

Acknowledgement

This work was supported by the National Natural Science Foundation of China (Grant No. 21304064), the Natural Science Foundation of Jiangsu Province (Grant No. BK20130292) and a Project Funded by the Priority Academic Program Development of Jiangsu Higher Education Institutions (PAPD) and the Fund for Excellent Creative Research Teams of Jiangsu Higher Education Institutions. CYL is grateful for the support from the National Science Foundation through grants CMMI-1100166 and DMR-1308958.

Notes and references

^a Institute of Functional Nano & Soft Materials (FUNSOM) & Collaborative Innovation Center for Suzhou Nano Science and Technology, Jiangsu Key Laboratory for Carbon-Based Functional Materials & Devices, Soochow University, Suzhou 215123 (P. R. China). E-mail: bdong@suda.edu.cn

^b Department of Materials Science and Engineering, Drexel University, Philadelphia, PA 19104 (USA) E-mail: chrisli@drexel.edu

† Electronic Supplementary Information (ESI) available: Experimental section, Fig. S1-S8 and Video S1-S4. See DOI: 10.1039/c000000x/

- G. A. Ozin, I. Manners, S. Fournier-Bidoz and A. Arsenault, *Adv. Mater.*, 2005, **17**, 3011-3018.
- J. Wang, *ACS Nano*, 2009, **3**, 4-9.
- T. Mirkovic, N. S. Zacharia, G. D. Scholes and G. A. Ozin, *ACS Nano*, 2010, **4**, 1782-1789.
- J. Wang and W. Gao, *ACS Nano*, 2012, **6**, 5745-5751.
- D. Patra, S. Sengupta, W. T. Duan, H. Zhang, R. Pavlick and A. Sen, *Nanoscale*, 2013, **5**, 1273-1283.
- R. F. Ismagilov, A. Schwartz, N. Bowden and G. M. Whitesides, *Angew. Chem. Int. Ed.*, 2002, **41**, 652-654.
- W. F. Paxton, K. C. Kistler, C. C. Olmeda, A. Sen, S. K. St Angelo, Y. Y. Cao, T. E. Mallouk, P. E. Lammert and V. H. Crespi, *J. Am. Chem. Soc.*, 2004, **126**, 13424-13431.
- T. R. Kline, W. F. Paxton, T. E. Mallouk and A. Sen, *Angew. Chem. Int. Ed.*, 2005, **44**, 744-746.
- J. Burdick, R. Laocharoensuk, P. M. Wheat, J. D. Posner and J. Wang, *J. Am. Chem. Soc.*, 2008, **130**, 9164-9165.
- A. A. Solovev, Y. F. Mei, E. B. Urena, G. S. Huang and O. G. Schmidt, *Small*, 2009, **5**, 1688-1692.
- S. Sundararajan, P. E. Lammert, A. W. Zudans, V. H. Crespi and A. Sen, *Nano Lett.*, 2008, **8**, 1271-1276.
- W. Gao, S. Sattayasamitsathit, J. Orozco and J. Wang, *J. Am. Chem. Soc.*, 2011, **133**, 11862-11864.
- S. Balasubramanian, D. Kagan, C. M. J. Hu, S. Campuzano, M. J. Lobo-Castanon, N. Lim, D. Y. Kang, M. Zimmerman, L. F. Zhang and J. Wang, *Angew. Chem. Int. Ed.*, 2011, **50**, 4161-4164.
- R. Liu and A. Sen, *J. Am. Chem. Soc.*, 2011, **133**, 20064-20067.
- R. A. Pavlick, S. Sengupta, T. McFadden, H. Zhang and A. Sen, *Angew. Chem. Int. Ed.*, 2011, **50**, 9374-9377.
- W. Gao, M. D'Agostino, V. Garcia-Gradilla, J. Orozco and J. Wang, *Small*, 2013, **9**, 467-471.
- F. Z. Mou, C. R. Chen, H. R. Ma, Y. X. Yin, Q. Z. Wu and J. G. Guan, *Angew. Chem. Int. Ed.*, 2013, **52**, 7208-7212.
- W. Gao, D. Kagan, O. S. Pak, C. Clawson, S. Campuzano, E. Chuluun-Erdene, E. Shipton, E. E. Fullerton, L. F. Zhang, E. Lauga and J. Wang, *Small*, 2012, **8**, 460-467.
- Y. J. Wu, Z. G. Wu, X. K. Lin, Q. He and J. B. Li, *ACS Nano*, 2012, **6**, 10910-10916.
- Z. G. Wu, Y. J. Wu, W. P. He, X. K. Lin, J. M. Sun and Q. He, *Angew. Chem. Int. Ed.*, 2013, **52**, 7000-7003.
- M. Guix, J. Orozco, M. Garcia, W. Gao, S. Sattayasamitsathit, A. Merkoci, A. Escarpa and J. Wang, *ACS Nano*, 2012, **6**, 4445-4451.
- L. Soler, V. Magdanz, V. M. Fomin, S. Sanchez and O. G. Schmidt, *ACS Nano*, 2013, **7**, 9611-9620.
- J. Orozco, G. Z. Cheng, D. Vilela, S. Sattayasamitsathit, R. Vazquez-Duhalt, G. Valdes-Ramirez, O. S. Pak, A. Escarpa, C. Y. Kan and J. Wang, *Angew. Chem. Int. Ed.*, 2013, **52**, 13276-13279.
- J. Orozco, V. Garcia-Gradilla, M. D'Agostino, W. Gao, A. Cortes and J. Wang, *ACS Nano*, 2013, **7**, 818-824.
- D. Kagan, P. Calvo-Marzal, S. Balasubramanian, S. Sattayasamitsathit, K. M. Manesh, G. U. Flechsig and J. Wang, *J. Am. Chem. Soc.*, 2009, **131**, 12082-12083.
- J. Wu, S. Balasubramanian, D. Kagan, K. M. Manesh, S. Campuzano and J. Wang, *Nat. Commun.*, 2010, **1**, 36.
- V. Garcia-Gradilla, J. Orozco, S. Sattayasamitsathit, F. Soto, F. Kuralay, A. Pourazary, A. Katzenberg, W. Gao, Y. F. Shen and J. Wang, *ACS Nano*, 2013, **7**, 9232-9240.
- B. Dong, T. Zhou, H. Zhang and C. Y. Li, *ACS Nano*, 2013, **7**, 5192-5198.
- B. Dong, D. L. Miller and C. Y. Li, *J. Phys. Chem. Lett.*, 2012, **3**, 1346-1350.
- B. Dong, W. D. Wang, D. L. Miller and C. Y. Li, *J. Mater. Chem.*, 2012, **22**, 15526-15529.
- J. C. Love, L. A. Estroff, J. K. Kriebel, R. G. Nuzzo and G. M. Whitesides, *Chem. Rev.*, 2005, **105**, 1103-1169.
- T. A. Taton, C. A. Mirkin and R. L. Letsinger, *Science*, 2000, **289**, 1757-1760.
- Y. W. C. Cao, R. C. Jin and C. A. Mirkin, *Science*, 2002, **297**, 1536-1540.
- S. Gupta, S. Huda, P. K. Kilpatrick and O. D. Velev, *Anal. Chem.*, 2007, **79**, 3810-3820.
- J. H. He, I. Ichinose, T. Kunitake and A. Nakao, *Langmuir*, 2002, **18**, 10005-10010.
- C. M. Welch, C. E. Banks, A. O. Simm and R. G. Compton, *Anal. Bioanal. Chem.*, 2005, **382**, 12-21.
- B. Zhao, Z. R. Liu, Z. L. Liu, G. X. Liu, Z. Li, J. X. Wang and X. T. Dong, *Electrochem. Commun.*, 2009, **11**, 1707-1710.
- H. Wang, G. J. Zhao and M. Pumera, *J. Am. Chem. Soc.*, 2014, **136**, 2719-2722.
- A. A. Solovev, W. Xi, D. H. Gracias, S. M. Harazim, C. Deneke, S. Sanchez and O. G. Schmidt, *ACS Nano*, 2012, **6**, 1751-1756.
- K. M. Manesh, M. Cardona, R. Yuan, M. Clark, D. Kagan, S. Balasubramanian and J. Wang, *ACS Nano*, 2010, **4**, 1799-1804.
- W. Gao, X. M. Feng, A. Pei, Y. E. Gu, J. X. Li and J. Wang, *Nanoscale*, 2013, **5**, 4696-4700.
- Z. H. Gan, Q. Z. Liang, J. Zhang and X. B. Jing, *Polym. Degrad. Stab.*, 1997, **56**, 209-213.
- Z. H. Gan, D. H. Yu, Z. Y. Zhong, Q. Z. Liang and X. B. Jing, *Polymer*, 1999, **40**, 2859-2862.
- T. Iwata and Y. Doi, *Polym. Int.*, 2002, **51**, 852-858.
- G. J. Zhao, B. Khezri, S. Sanchez, O. G. Schmidt, R. D. Webster and M. Pumera, *Chem. Commun.*, 2013, **49**, 9125-9127.
- D. Kagan, M. J. Benchimol, J. C. Claussen, E. Chuluun-Erdene, S. Esener and J. Wang, *Angew. Chem. Int. Ed.*, 2012, **51**, 7519-7522.
- A. Breier and A. Ziegelhofer, *Gen. Physiol. Biophys.*, 2000, **19**, 253-263.
- I. S. M. Khalil, V. Magdanz, S. Sanchez, O. G. Schmidt and S. Misra, *PLoS One*, 2014, **9**, e83053.
- J. Wang and K. M. Manesh, *Small*, 2010, **6**, 338-345.